

Probing spatially resolved spin density correlations with trapped excitons

Shanshan Ding,^{1,2} Jose Antonio Valerrama Botia,^{1,3} Aleksi Julku,¹ Zhigang Wu,³ and G. M. Bruun⁴

¹*Center for Complex Quantum Systems, Department of Physics and Astronomy,
Aarhus University, Ny Munkegade, DK-8000 Aarhus C, Denmark*

²*Institute of Atomic and Molecular Physics, Sichuan University, Chengdu 610065, China*

³*Quantum Science Center of Guangdong-Hong Kong-Macao Greater Bay Area (Guangdong), Shenzhen 508045, China*

⁴*Department of Physics and Astronomy, Aarhus University, Ny Munkegade, DK-8000 Aarhus C, Denmark*

(Dated: December 17, 2025)

The rapidly growing class of atomically thin and tunable van der Waals materials is intensely investigated both in the context of fundamental science and for new technologies. There is in this connection a widespread need for new ways to probe the electronic properties of these layered materials, since their two-dimensional (2D) character make conventional probes less efficient. Here, we show how excitons trapped in a moiré lattice can be used as an optical probe for spatially resolved electron spin density correlations in such materials. The electrons in the material of interest virtually tunnel to the moiré lattice where they scatter on the excitons after which they tunnel back. This gives rise to an effective spin-dependent and spatially localised potential felt by the electrons, which in turn leads to energy shifts that can be measured spectroscopically in the exciton spectrum. Using second order perturbation theory combined with a solution to the exciton-electron scattering problem, we show that the electrons mediate an interaction between two excitons resulting in an energy shift proportional to their two-point spin density-density correlation function evaluated at the exciton positions. We then discuss two specific applications of our setup. First, we show that quantum phase transitions between different in-plane anti-ferromagnetic orders in a 2D lattice give rise to large and measurable shifts in the exciton spectrum in the critical regions. Second, we analyse how different pairing symmetries of superconducting phases can be probed. This demonstrates that our scheme opens up new ways to probe electron spin density correlations, which is a key property of many quantum phases predicted to exist in the new 2D materials.

I. INTRODUCTION

The increasingly sophisticated fabrication of atomically thin transition metal dichalcogenides (TMDs) MX_2 (e.g. M=Mo or W and X=S, Se or Te) and their heterostructures have resulted in an increasing number of new and interesting 2D quantum materials¹. TMDs are direct band gap semiconductors that have band extrema at the so-called K and K' points in their hexagonal Brillouin zone with a large spin-valley splitting, where each valley can be selectively excited using circularly polarized light^{2,3}. The reduced screening of the Coulomb interaction in these 2D materials combined with their typically large electron and hole band masses lead to large interaction-to-kinetic energy ratios. One can moreover stack TMDs on top of each other with a lattice mismatch or with a relative twist angle and in this way create a moiré superlattice potential with almost flat electronic bands in the reduced Brillouin zone. Many properties of these moiré systems can be tuned such as their carrier density and ratio of interaction energy to hopping strength, in order to realise new quantum many-body phases of interest for fundamental science and technological applications^{4–8}. A major problem however is that transport spectroscopy, which is often used to probe strongly correlated systems, has proven difficult to implement for these materials. Likewise, their layered structure makes them couple only weakly to X-ray and neutron spectroscopic probes. All this means that there is a widespread need for alternative ways to probe the new

2D materials.

One possibility is to use excitons as an optical probe for the electronic states of the 2D materials. The general idea is that interactions with the electrons change the optical spectrum of the excitons in ways that depend on the state of the electrons such as whether it is gapped or not. This has been utilized to detect the formation of a Wigner crystal^{9,10}, incompressible Mott states¹¹, spin ordering in a triangular moiré lattice¹², and a range of correlated phases^{13–16}. The presence of quasiparticle peaks in the exciton spectrum was used to identify incompressible filled Landau levels in graphene¹⁷, quantum Hall states in TMDs¹⁸, and exciton insulators in a moiré lattice¹⁹. Theoretically, it has been analysed how different electronic phases show up in the exciton spectrum^{20–24}. For a recent review discussing excitons as probes for 2D materials, see Ref. 25.

Recently, resonant scattering between charge carriers in one layer and excitons in another due to virtual tunneling has been observed experimentally²⁶, and this scattering process has been predicted to lead to magnetic polarons and string excitations for a mobile exciton²¹. Inspired by these results, we explore in this paper how density correlations in a 2D material can be probed in the optical spectrum of excitons trapped in an adjacent moiré lattice. Electrons from the material of interest tunnel virtually into the moiré lattice, where they scatter on the excitons before tunneling back. Since an electron mainly scatters on an exciton with opposite spin, this gives rise to an effective, spin-dependent static potential for the electrons in the material. We show that this can be used

to measure the two-point spin density correlation function of the electrons via the second order energy shift of the excitons. Using two excitons separated by a distance, the spatial dependence of the correlation function can be probed. Two specific examples of this are then discussed. We first demonstrate how the quantum phase transitions between different in-plane anti-ferromagnetic orders in a 2D spin lattice give rise to a large signal in the exciton spectrum in the critical regions. Then we show how the spatial symmetry of the Cooper pairs in different superconducting phases can be probed using two excitons.

II. SYSTEM

We consider the setup illustrated in Fig. 1. An upper system contains two excitons at positions \mathbf{r}_1 and \mathbf{r}_2 , as can be achieved experimentally by trapping them in a deep moiré lattice^{27–29}. The excitons have spins $\bar{\sigma}_1$ and $\bar{\sigma}_2$ meaning that they are formed by a spin $\bar{\sigma} = \uparrow, \downarrow$ electron excited from a valance to a conduction band, which can be realised using the spin-valley locking of TMDs¹. A lower system contains electrons whose properties we aim to probe with the excitons. In the following, we refer to the upper and lower 2D systems as two layers even though they each typically consist of two or more layers forming moiré lattices as in the examples we will consider below. We also refer to the charge carriers as electrons but they may be holes as well. An insulating spacing material, such as hexagonal Boron Nitride (hBN), separates the two layers thereby prohibiting the formation of a moiré system or other hybridisation effects, while at the same time allowing for electron tunneling between the two layers. The Hamiltonian is

$$\hat{H} = \sum_{\mathbf{k}\sigma} (\epsilon_{\mathbf{k}} + \delta) \hat{a}_{\mathbf{k}\sigma}^\dagger \hat{a}_{\mathbf{k}\sigma} + \hat{H}_e + t_{\perp} \sum_{\mathbf{k}\sigma} (\hat{a}_{\mathbf{k}\sigma}^\dagger \hat{c}_{\mathbf{k}\sigma} + \text{h.c.}) + \frac{1}{N} \sum_{i=1}^2 \sum_{\mathbf{k}, \mathbf{k}'} e^{i(\mathbf{k}' - \mathbf{k}) \cdot \mathbf{r}_i} V_{\text{ex}}(\mathbf{k} - \mathbf{k}') \hat{a}_{\mathbf{k}\sigma_i}^\dagger \hat{a}_{\mathbf{k}'\sigma_i}, \quad (1)$$

where $\hat{a}_{\mathbf{k}\sigma}^\dagger / \hat{c}_{\mathbf{k}\sigma}^\dagger$ creates an electron in the upper/lower layer, \hat{H}_e is the Hamiltonian for the electrons in the lower layer, σ is the opposite spin of $\bar{\sigma}$, and N is the number of lattice sites in the upper layer where the excitons are trapped. The energy of an electron in the upper layer with crystal momentum \mathbf{k} is $\epsilon_{\mathbf{k}} + \delta$ where δ is an energy off-set with respect to the lower layer, which can be controlled by gating. We have assumed that there is only a significant interaction $V_{\text{ex}}(\mathbf{k})$ excitons with opposite spins in the upper layer, since the interaction between electrons and excitons with parallel spins is strongly suppressed by the Pauli exclusion principle²⁵. In particular, only the interaction between electrons and excitons with opposite spins support a bound state, i.e. a trion, a property that will be used extensively below. Finally, we have for simplicity assumed that the electron tunneling between the two layers with matrix element t_{\perp} conserves crystal

momentum, which strictly speaking only holds when the (moiré) lattices in the upper and lower layers are identical. In App. A we show that when the lattice constants a_1 and a_2 of the two layers differ, the momentum can change by multiples of $\Delta\mathbf{k} \propto 1/a_1 - 1/a_2$ in the tunneling process. For a small lattice mismatch, these effects are however negligible so that the dominant tunneling process indeed conserves the in plane momentum.

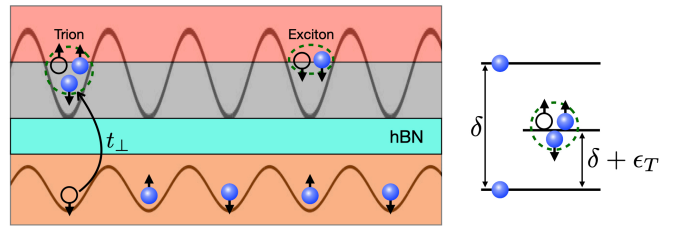


FIG. 1. Electrons (blue balls) in the lower material can tunnel to the upper material, where they scatter on excitons with opposite spin trapped by a deep moiré potential. The exciton-electron interaction potential supports a bound state, i.e. a trion. The energy levels of the electron in the lower material as well as of the electron and trion in the upper material are shown on the right.

III. EFFECTIVE STATIC POTENTIAL

We now show how the scattering of electron on an exciton in the upper layer gives rise to an effective static potential felt by the electrons in the lower layer. For this purpose, consider the scattering of an electron in the upper layer on a static exciton with opposite spin. The electron-exciton scattering matrix obeys the Lippmann–Schwinger equation [see Fig. 2(a)]

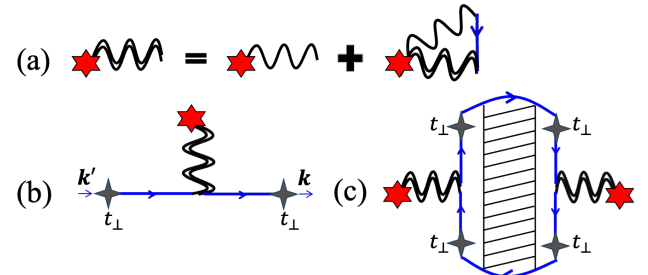


FIG. 2. (a) Diagrams for electron-exciton scattering matrix in the upper layer. (b) Self-energy of the electrons in the lower layer due to tunneling to the upper layer, scattering on the exciton, and tunneling back. (c) The interaction between two excitons mediated by electrons in the lower layer. Red stars (grey crosses) represent the static exciton (tunneling between two layers), single (double) wavy lines are the bare electron-exciton interaction (electron-exciton scattering matrix), and the blue lines are the propagator for the electron.

$$\begin{aligned} \mathcal{T}(\mathbf{k}, \mathbf{k}', \omega) &= V_{\text{ex}}(\mathbf{k} - \mathbf{k}') \\ &+ \frac{1}{N} \sum_{\mathbf{k}''} V_{\text{ex}}(\mathbf{k} - \mathbf{k}'') G_U(\mathbf{k}'', \omega) \mathcal{T}(\mathbf{k}'', \mathbf{k}'; \omega), \end{aligned} \quad (2)$$

where \mathbf{k}/\mathbf{k}' is the outgoing/incoming momentum of the electron, ω is the scattering energy, $G_U(\mathbf{k}, \omega) = 1/(\omega - \epsilon_{\mathbf{k}} - \delta)$ is the Green's function for an electron in the upper layer, and we have for notational simplicity taken the exciton to be located at the origin ($\mathbf{r}_i = 0$). We assume that the electron can bind the exciton to form a moiré trapped trion with energy $\epsilon_T < 0$ relative to the exciton energy as observed experimentally³⁰⁻³². It follows that the scattering matrix diverges at the energy $\omega = \delta + \epsilon_T$. For a short range electron-exciton interaction this can be used to replace $V_{\text{ex}}(\mathbf{k})$ with the trion energy in the Lippmann-Schwinger equation²⁵. We can to a good approximation ignore the frequency dependence of the scattering matrix for $\omega \ll \delta + \epsilon_T$, which together with $G_U(\mathbf{k}, \omega) \simeq -1/\delta$ means that the solution to the Lippmann-Schwinger equation is

$$\mathcal{T}(\mathbf{k}, \mathbf{k}', \omega) \simeq \frac{\epsilon_T \delta}{\delta + \epsilon_T}. \quad (3)$$

Details of this derivation are given in App. B. When the exciton is located at position \mathbf{r}_i away from the origin, the scattering matrix in Eq. (3) is simply multiplied by a factor $e^{i(\mathbf{k}' - \mathbf{k}) \cdot \mathbf{r}_i}$. Note that Eq. (3) breaks down when the energy ω of the electron is close to that of the trion $\epsilon_T + \delta$, which gives rise to resonant scattering with a strong energy dependence, see App. B.

We can now calculate the static potential experienced by spin σ electrons in the lower layer due to an exciton in the upper layer with opposite spin $\bar{\sigma}$ located at \mathbf{r}_i . The tunneling between the two layers gives rise to a self-energy term for σ electrons in the lower layer of the form

$$\begin{aligned} \Sigma(\mathbf{k}, \mathbf{k}', \omega) &= t_{\perp}^2 G_U(\mathbf{k}, \omega) \mathcal{T}(\mathbf{k}, \mathbf{k}', \omega) G_U(\mathbf{k}', \omega) \\ &+ t_{\perp}^2 G_U(\mathbf{k}, \omega) \delta_{\mathbf{k}, \mathbf{k}'}. \end{aligned} \quad (4)$$

Physically, Eq. (4) describes a spin σ electron with crystal momentum \mathbf{k}' in the lower layer tunneling to the upper layer where it scatters on the $\bar{\sigma}$ exciton to momentum \mathbf{k} after which it tunnels down to the lower layer again as illustrated diagrammatically in Fig. 2(b). The second term in Eq. (4) corresponds to free electron propagation in the upper layer without scattering, which gives a constant energy shift that is omitted in the following.

Assuming again that the typical energy ω of the electrons in the lower layer is far detuned from the scattering resonance, i.e., $\omega \ll \delta + \epsilon_T$, the energy/moment dependence of scattering matrix can be ignored so that it is given by Eq. (3). Using this together with $G_U(\mathbf{k}, \omega) \simeq -1/\delta$, the self-energy in Eq. (4) reduces to that coming

from a static scattering potential given by

$$\begin{aligned} \hat{V}_{\text{eff}}(\mathbf{r}_i) &= \frac{t_{\perp}^2}{\delta^2} \frac{\epsilon_T \delta}{\delta + \epsilon_T} \frac{1}{N} \sum_{\mathbf{k}, \mathbf{k}'} e^{i(\mathbf{k}' - \mathbf{k}) \cdot \mathbf{r}_i} \hat{c}_{\mathbf{k}\sigma}^{\dagger} \hat{c}_{\mathbf{k}'\sigma} \\ &= \frac{t_{\perp}^2}{\delta} \frac{\epsilon_T}{\delta + \epsilon_T} \hat{c}_{i\sigma}^{\dagger} \hat{c}_{i\sigma} = \kappa \hat{n}_{\sigma}(\mathbf{r}_i). \end{aligned} \quad (5)$$

Here, $\hat{c}_{i\sigma}^{\dagger} = N^{-1/2} \sum_{\mathbf{k}} e^{-i\mathbf{k} \cdot \mathbf{r}_i} \hat{c}_{\mathbf{k}\sigma}^{\dagger}$ creates a spin σ electron at position \mathbf{r}_i , and $\hat{n}_{\sigma}(\mathbf{r}_i) = \hat{c}_{i\sigma}^{\dagger} \hat{c}_{i\sigma}$ is the density of σ electrons at position \mathbf{r}_i . Consistent with assuming momentum conservation in the tunneling between the layers, we have taken the lattices in two layers to be identical when performing the Fourier transformation. Equation (5) shows that a spin $\bar{\sigma}$ exciton at position \mathbf{r}_i in the upper layer gives rise to a local potential experienced by the spin σ electrons in the lower layer with a strength $\kappa = t_{\perp}^2 \epsilon_T / [\delta(\delta + \epsilon_T)]$. We emphasize that the same scattering process as that considered here involving virtual tunneling of charge carriers in one layer to another layer containing an exciton has recently been experimentally realised^{26,33}. In this case, resonant hole-exciton scattering was achieved by tuning the energy offset between the layers to cancel the trion energy, which corresponds to setting $\epsilon_T + \delta = 0$ in the present case.

IV. PROBING SPIN DENSITY CORRELATIONS

Having derived the effective static potential felt by electrons in the lower layer due to trapped excitons in the upper layer, we will in this section show how this can be used to realise an optical probe of spin density correlations of the electrons.

Consider first a single exciton at position \mathbf{r}_1 in the upper layer with spin $\bar{\sigma}$. This leads to a local potential given by Eq. (5) for the spin σ electrons below. Assuming that this potential is weak, the resulting energy shift can be calculated using perturbation theory. The first order energy shift at zero temperature is given by the mean-field expression

$$E_1 = \langle \psi_0 | \hat{V}_{\text{eff}} | \psi_0 \rangle = \kappa n_{\sigma}(\mathbf{r}_1), \quad (6)$$

where $|\psi_0\rangle$ is the many-body ground state of the electrons in the lower layer with spin density $n_{\sigma}(\mathbf{r}_1) = \langle \psi_0 | \hat{n}_{\sigma}(\mathbf{r}_1) | \psi_0 \rangle$. This shows that the energy shift of the exciton can be used to measure spin resolved densities in the lower layer. For instance, an out-of-plane ferromagnetic order can be detected spectroscopically as an exciton energy shift depending on its spin, and an out-of-plane anti-ferromagnetic order will show up as an energy shift oscillating as a function of the exciton position. For a non-zero temperature, we can simply replace $\langle \psi_0 | \dots | \psi_0 \rangle$ in Eq. (6) by a thermal average $\langle \dots \rangle$.

Probing the spin density *correlations* of electrons, which often provide smoking gun signals of their quantum state, remains a major challenge for 2D materials.

We now show how this can be achieved by measuring the second order energy shift of the excitons. Consider two excitons at positions \mathbf{r}_i with spins $\bar{\sigma}_i$ ($i = 1, 2$) giving rise to a first order energy shift $E_1 = \kappa n_{\sigma_1}(\mathbf{r}_1) + \kappa n_{\sigma_2}(\mathbf{r}_2)$. The second order shift is

$$\begin{aligned} E_2 &= \sum_{n>0} \frac{|\langle \psi_n | \hat{V}_{\text{eff}}(\mathbf{r}_1) + \hat{V}_{\text{eff}}(\mathbf{r}_2) | \psi_0 \rangle|^2}{E_0 - E_n} \\ &= -\frac{\kappa^2}{2} [\langle \langle \hat{n}_{\sigma_1}(\mathbf{r}_1), \hat{n}_{\sigma_1}(\mathbf{r}_1) \rangle \rangle + \langle \langle \hat{n}_{\sigma_2}(\mathbf{r}_2), \hat{n}_{\sigma_2}(\mathbf{r}_2) \rangle \rangle] \\ &\quad - \kappa^2 \langle \langle \hat{n}_{\sigma_1}(\mathbf{r}_1), \hat{n}_{\sigma_2}(\mathbf{r}_2) \rangle \rangle, \end{aligned} \quad (7)$$

where $|\psi_n\rangle$ is an eigenstate of the electron system with energy E_n and E_0 is the ground state energy. Here, $\langle \langle \hat{A}, \hat{B} \rangle \rangle$ denotes the zero frequency component of the retarded correlation function

$$\langle \langle \hat{A}, \hat{B} \rangle \rangle(t) = -i\theta(t) \langle [\hat{A}(t), \hat{B}(0)] \rangle \quad (8)$$

where $\hat{O}(t) = e^{i\hat{H}_e t} \hat{O} e^{-i\hat{H}_e t}$ is a time-dependent operator in the Heisenberg representation with respect to the many-body Hamiltonian of the electrons in the lower layer, see App. C.

Equation (7) shows that the second order energy shift of the two excitons is proportional to the sum of spin resolved density-density correlations of the electrons. It follows that one can probe the spatial and spin dependence of the electron density correlations in a material of interest using optical spectroscopy of excitons. The appearance of $\langle \langle \hat{n}_{\sigma_1}(\mathbf{r}_1), \hat{n}_{\sigma_2}(\mathbf{r}_2) \rangle \rangle$ can be interpreted as the interaction between the two excitons in the top layer mediated by the electrons in the lower layer as illustrated diagrammatically in Fig. 2(c). A similar approach has been used to derive the interaction between static ions and neutral particles in ultracold atomic gases^{34,35}. Equation (7) can straightforwardly be generalised to the case of an arbitrary number of excitons at positions \mathbf{r}_i in the lattice.

V. PROBING MAGNETIC PHASES

We now consider a specific use case of our setup: probing spin correlations in different magnetic phases of electron lattice systems. Consider a half filled lattice with strong on-site repulsion between the electrons so that their low energy spin degrees of freedom are described by a Heisenberg model³⁶. Since there is one electron per site, we can write $\hat{n}_\sigma(\mathbf{r}_i) = 1/2 + \sigma \hat{S}_z(\mathbf{r}_i)$ where $\hat{\mathbf{S}}(\mathbf{r}_i) = [\hat{S}_x(\mathbf{r}_i), \hat{S}_y(\mathbf{r}_i), \hat{S}_z(\mathbf{r}_i)]$ is the vector operator for the spin at position \mathbf{r}_i and $\sigma = \pm$ for spin \uparrow / \downarrow in this section. It immediately follows that

$$\langle \langle \hat{n}_{\sigma_i}(\mathbf{r}_i), \hat{n}_{\sigma_j}(\mathbf{r}_i) \rangle \rangle = \sigma_i \sigma_j \langle \langle \hat{S}_z(\mathbf{r}_i), \hat{S}_z(\mathbf{r}_j) \rangle \rangle, \quad (9)$$

which together with Eq. (7) demonstrates that our scheme is well-suited for probing the spin correlations.

Take as a concrete example a lower system consisting of a twisted bilayer WSe₂, which in the strong repulsion limit and at half filling is described by the spin model^{6,7}

$$\begin{aligned} \hat{H}_S &= J \sum_{\langle i,j \rangle} \{ \hat{S}_z(\mathbf{r}_i) \hat{S}_z(\mathbf{r}_j) + \cos 2\phi_{ij} [\hat{S}_x(\mathbf{r}_i) \hat{S}_x(\mathbf{r}_j) \\ &\quad + \hat{S}_y(\mathbf{r}_i) \hat{S}_y(\mathbf{r}_j)] + \sin 2\phi_{ij} [\hat{\mathbf{S}}(\mathbf{r}_i) \times \hat{\mathbf{S}}(\mathbf{r}_j)] \cdot \hat{z} \} \end{aligned} \quad (10)$$

on a triangular lattice. Here, $J > 0$ is the superexchange coupling between neighbouring spins and the phase ϕ_{ij} is symmetric under $2\pi/3$ rotations with $\phi_{ij} = -\phi_{ji}$. For convenience, we define $\phi_{ij} = \phi$ for the phase between a spin at site i and the nearest neighbour spin j in the horizontal (x) direction. The ground state of \hat{H}_S is a $120^\circ - 2$ in-plane antiferromagnet, an in-plane ferromagnet, and a $120^\circ - 1$ in-plane antiferromagnet when $\phi \in [0, \pi/3]$, $[\pi/3, 2\pi/3]$, and $[2\pi/3, \pi]$ respectively⁷, as illustrated in Fig. 3. Since the magnetic order is in-plane, the first order energy shift Eq. (6) will be the same for all three phases. In order to distinguish them, we therefore focus on the second order energy shift given by Eq. (7).

The spin-spin correlation function is within linear spin-wave theory given by

$$\langle \langle \hat{S}_z(\mathbf{r}_i), \hat{S}_z(\mathbf{r}_j) \rangle \rangle = \frac{1}{NJ} \sum_{\mathbf{k}} \frac{e^{i\mathbf{k} \cdot (\mathbf{r}_i - \mathbf{r}_j)}}{A_{\mathbf{k}} + B_{\mathbf{k}}} \quad (11)$$

for the in-plane ferromagnetic phase. Here

$$A_{\mathbf{k}} = -6 \cos 2\phi + (\cos 2\phi + 1) \gamma_{\mathbf{k}}, \quad (12)$$

$$B_{\mathbf{k}} = -(\cos 2\phi - 1) \gamma_{\mathbf{k}}, \quad (13)$$

$$\gamma_{\mathbf{k}} = \cos k_x + 2 \cos(k_x/2) \cos(\sqrt{3}k_y/2), \quad (14)$$

and we have taken the lattice constant to be unity. The spin-spin correlation functions for the $120^\circ - 1$ and $120^\circ - 2$ antiferromagnetic phases are same as above except for a shift of the angle ϕ by $\pm\pi/3$. Details of deriving Eqs. (11)-(14) are given in App. D.

The blue line in Fig. 3 shows the second order energy shift of a single exciton as a function of the angle ϕ given by Eq. (7) and Eq. (9) without the terms involving $n_{\sigma_2}(\mathbf{r}_2)$, where we have evaluated Eq. (11) numerically. Figure 3 shows that interactions of the exciton with the electrons below give rise to a negative second order energy shift of the order κ^2/J . We also see that the energy shift increases as the transitions between the different anti-ferromagnetic phases are approached, and that it diverges at the critical points. These divergencies arise because the different phases differ by spin rotations of the spins in the xy -plane, which is generated by \hat{S}_z , or equivalently because \hat{S}_z excites spin waves of the magnet, which become soft at the phase transition points. Of course, second order perturbation theory is inaccurate for such large energy shifts and a non-perturbative approach is therefore needed in the critical regions to get quantitatively accurate results. The result that magnetic phase transitions give rise to a large signal in the exciton spectrum is nevertheless robust, since the excitons probe

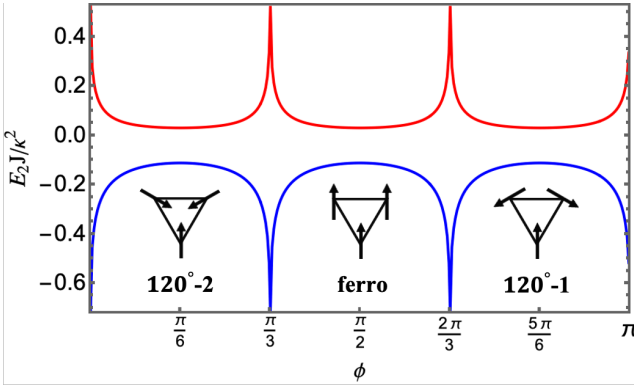


FIG. 3. The second order energy shift of the spin model given by Eq. (10) due to the excitons in the upper layer. The blue line represents the result for one exciton and the red line shows the interaction term between two nearest neighbour excitons with the same spin.

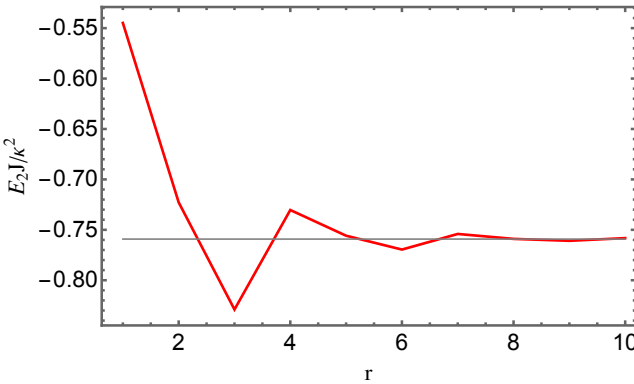


FIG. 4. The second order energy shift for two excitons with parallel spins in the upper layer as a function of their separation r in units of the lattice constant with $\phi = 0.34\pi$.

spin-spin correlation functions that typically diverge at the critical points.

Consider now two excitons with parallel spins located at nearest neighbour lattice sites \mathbf{r}_1 and \mathbf{r}_2 . The red line in Fig. 3 shows the $\mathbf{r} = \mathbf{r}_1 - \mathbf{r}_2$ dependent term of the second order energy shift of two excitons given by the last term in Eq. (7) proportional to $\langle\langle \hat{S}_z(\mathbf{r}_1), \hat{S}_z(\mathbf{r}_2) \rangle\rangle$. This shows that the interaction between two nearest neighbour excitons with parallel spins mediated by the spins is repulsive and that it also diverges at the phase transitions. To examine the spatial dependence further, we plot in Fig. 4 the energy shift of the two excitons as a function of their separation r . We have taken $\phi = 0.34\pi$ so that the system is in the ferromagnetic phase close to the transition point to the anti-ferromagnetic $120^\circ - 2$ phase, see Fig. 3. The energy shift due to the interaction mediated by spin waves oscillates as a function of the distance between the two excitons akin to the Friedel oscillations of the Ruderman-Kittel-Kasuya-Yosida (RKKY) interaction³⁷⁻³⁹. For large distance $r \gg 1$ between the two excitons, the energy shift reduces to that of two isolated

excitons (grey line) as expected. By measuring these oscillations, one can therefore probe the spatial dependence of the spin-spin correlations of the electrons or equivalently the spin-wave mediated interaction. The energy shift has a similar behaviour for other values of ϕ with the overall magnitude increasing the closer the system is to a critical point separating two magnetic phases.

Taking experimentally realistic values for the spin coupling $J = 0.05\text{meV}$ ⁴⁰ and the trion energy $\epsilon_T = -5\text{meV}$ ³⁰⁻³², assuming the energy off-set between the two layers is $\delta = 5.5\text{meV}$, and using $t_\perp = 1\text{meV}$ for the inter-layer tunneling matrix element, we get $\kappa^2/J \simeq 66\text{meV}$. This indicates that the energy shifts reported in Figs. 3-4 should be experimentally observable. From this we conclude that our setup can be applied to probe spin correlations of strongly correlated electrons in the Mott limit including their spatial dependence. This is useful since such correlations are a key property characterizing many strongly correlated phases also without magnetic order such as spin liquids⁴¹. Also, since magnetic phase transitions in general give rise to diverging spin-spin correlation functions they can be detected optically by a corresponding large energy shift in the exciton spectrum.

VI. PROBING SUPERCONDUCTING PHASES

As another application of our setup, we now explore the probing of different superconducting phases. Consider a simple BCS model for a nearest-neighbor tight-binding model on a triangular lattice with the Hamiltonian

$$\hat{H}_{\text{BCS}} = \sum_{\mathbf{k}\sigma} \xi_{\mathbf{k}} \hat{c}_{\mathbf{k}\sigma}^\dagger \hat{c}_{\mathbf{k}\sigma} + \sum_{\mathbf{k}} (\Delta_{\mathbf{k}} \hat{c}_{\mathbf{k}\uparrow}^\dagger \hat{c}_{-\mathbf{k}\downarrow}^\dagger + \text{h.c.}) \quad (15)$$

Here, $\xi_{\mathbf{k}} = -2t[\cos k_x + 2\cos(k_x/2)\cos(\sqrt{3}k_y/2)] - \mu$ is the tight binding kinetic energy for a triangular lattice with t the nearest neighbor hopping matrix element, μ the chemical potential of the electrons and $\Delta_{\mathbf{k}}$ the pairing strength between time-reversed electrons. Pairing will mainly affect the density correlations between opposite spin electrons, which show up in the density-density correlation functions entering Eq. (7). We find from a straightforward diagonalization of Eq. (15)(see App. E)

$$\langle\langle \hat{n}_\downarrow(\mathbf{r}_1), \hat{n}_\uparrow(\mathbf{r}_2) \rangle\rangle = \frac{1}{2N^2} \sum_{\mathbf{k}, \mathbf{k}'} \frac{\Delta_{-\mathbf{k}} \Delta_{\mathbf{k}'}^*}{E_{\mathbf{k}} + E_{\mathbf{k}'}} \frac{e^{-i(\mathbf{k}+\mathbf{k}') \cdot \mathbf{r}}}{E_{\mathbf{k}} E_{\mathbf{k}'}} \quad (16)$$

where $\mathbf{r} = \mathbf{r}_1 - \mathbf{r}_2$, $E_{\mathbf{k}} = \sqrt{\xi_{\mathbf{k}}^2 + |\Delta_{\mathbf{k}}|^2}$. Equation (16) shows as expected that Cooper pairing gives rise to density correlations between anti-parallel spins, which in turn can be probed via the resulting second order energy shift of two excitons with anti-parallel spins. From Eqs. (7) and (16) it follows that the energy shift scales as $\kappa^2 \Delta_{\text{BCS}}^2 / t^3$.

To demonstrate this, we consider two excitons with antiparallel spins separated by a distance r interacting

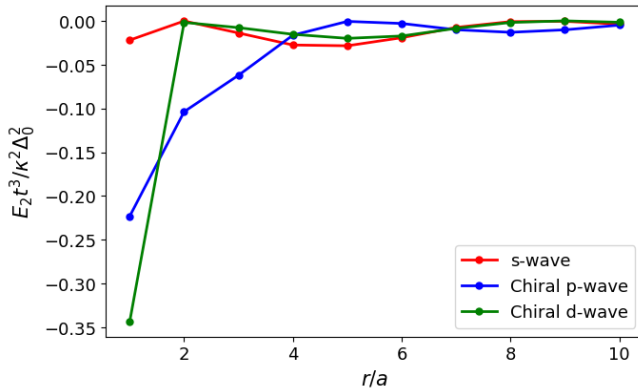


FIG. 5. The energy shift of two excitons with anti-parallel spins interacting with superconducting samples having three different kinds of Cooper pairing as a function of their separation. We have subtracted the energy shift when the excitons are infinitely apart.

with superconducting electrons in a triangular lattice. We choose three different kinds of pairings with the symmetry of the triangular lattice, namely⁴²

$$\frac{\Delta_{\mathbf{k}}}{\Delta_0} = \begin{cases} 1 & \text{s-wave} \\ 2i[\sin k_x + \cos(\sqrt{3}k_y/2)\sin(k_x/2)]/\sqrt{3} & \text{chiral} \\ +2\sin(\sqrt{3}k_y/2)\cos(k_x/2) & \text{p-wave} \\ 2[\cos k_x - \cos(k_x/2)\cos(\sqrt{3}k_y/2)]/\sqrt{3} & \text{chiral} \\ -2i\sin(\sqrt{3}k_y/2)\sin(k_x/2) & \text{d-wave} \end{cases}$$

where Δ_0 is the overall magnitude of the pairing.

Figure 5 shows the r -dependent part of the second order energy shift of two excitons with anti-parallel spins due to interactions with a superconductor with the pairing symmetries given above. We have for the numerical calculations taken $\Delta_0/t = 0.1$ and used a chemical potential $\mu/t = 0.83$ corresponding to an approximately half-filled (49.93%) lattice, where superconductivity has been observed both in twisted bilayer graphene and in twisted bilayer WSe₂^{43,44}. The energy shift is generally negative reflecting that Cooper pairing leads to positive density correlations between opposite spins. The spatial dependence of the energy shift is moreover determined by the gap function $\Delta_{\mathbf{k}}$ as quantified by Eq. (16).

To further illustrate how the spatial properties of the Cooper pairs can be probed, we plot in Fig. 6 the \mathbf{r} dependent part of the second order energy shift in the full lattice for *s*-wave pairing and *d*_{xy}-wave pairing with $\Delta_{\mathbf{k}} = 2\Delta_0 \sin(\sqrt{3}k_y/2)\sin(k_x/2)$. We have chosen the latter in order to showcase results for Cooper pairs breaking the underlying lattice symmetry. The plots clearly illustrate how the spatial structure of the Cooper pairs shows up in the dependence of the energy shift of the two excitons on their spatial separation.

To estimate the magnitude of the energy shifts in Figs. 5-6, we assume that the underlying band structure of the superconductor has a relatively small bandwidth of

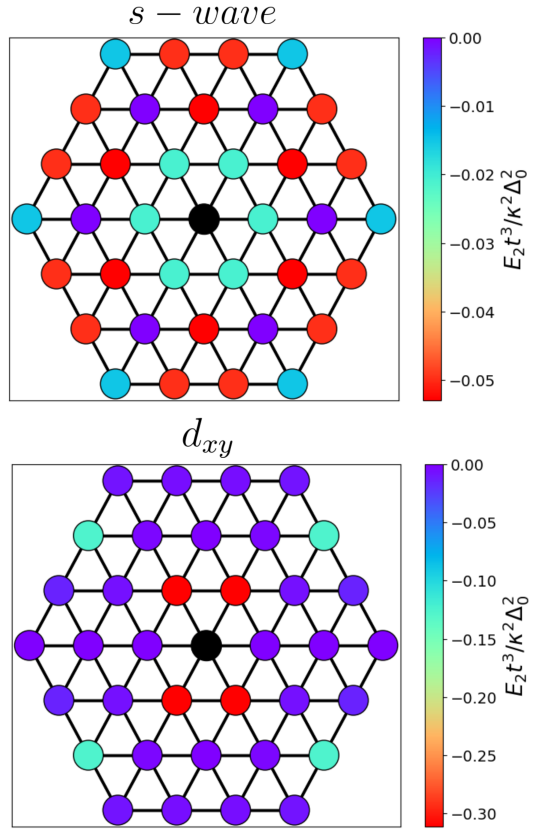


FIG. 6. The second order energy shift of two excitons with anti-parallel spins for a *s*-wave superconductor (top) and a *d*_{xy} superconductor (bottom). One exciton is at the origin (black dot) and the color codes give the energy shift when the other exciton is at a given lattice site. The energy shift when the two excitons are infinitely apart is subtracted.

5meV as in twisted bilayer graphene⁴⁴. Since the bandwidth in a triangular tight-binding model is $9t$, this corresponds to $t \simeq 0.56$ meV. Setting $\Delta_0/t = 0.1$ corresponding to a pairing strength 90 times smaller than the band width, and using the same values for the interlayer hopping $t_{\perp} = 1$ meV and the trion energy $\epsilon_T = -5$ meV as in Sec. V, we obtain $\kappa^2\Delta_0^2/t^3 \simeq 0.41$ meV for $\delta = 5.2$ meV. This makes the energy shifts reported in Figs. 5-6 at the limit of what can be observed. The magnitude of the energy shifts can of course be increased by tuning the energy off-set δ so that the exciton-electron scattering is closer to resonance. A reliable calculation of the energy shift in this regime however requires an extension of our theory to include the frequency dependence of the scattering omitted in Eq. (3). This is left for future work. These results indicate that our setup can be used to probe the properties of superconducting phases including the symmetry of the Cooper pairs. We have here used a minimal BCS Hamiltonian to demonstrate proof-of-concept of our scheme, and one should apply more realistic but also more complicated Hamiltonians to explore this in more detail for specific superconductors. Such models

should in particular include non-superfluid correlations between anti-parallel spins, which in general are present also in the absence of pairing.

VII. DISCUSSION AND OUTLOOK

We have demonstrated that excitons trapped in a moiré lattice can serve as an optical probe of electron spin density correlations in an adjacent 2D material. Virtual electron tunneling between the material and the moiré lattice combined with electron-exciton scattering gives rise to a spin-dependent static potential felt by the electrons in the 2D material. To second order, this in turn affects the energy by an amount proportional to the spin density-density correlation function of the electrons. By measuring the energy shift as a function of the separation between two excitons, one can therefore extract the spatial dependence of this correlation function, which can be interpreted as an interaction between the two excitons mediated by the electrons in the material. We then discussed two concrete applications of this setup: Detecting quantum phase transitions between different in-plane anti-ferromagnetic phases and measuring the spatial symmetry of Cooper pairs in different superconductors.

Our scheme can be implemented experimentally for instance by creating excitons in a moiré lattice with a certain concentration. This will give rise to a range of exciton spectral lines coming from excitons with different numbers of other excitons in their surroundings. These spectral lines may then be identified with e.g. a statistical analysis combined with theoretical modeling. Since the mediated interaction between two excitons generally decreases with their distance, it will likely in most cases be sufficient to consider exciton pairs separated by maximally a few lattice sites.

These results demonstrate that our scheme can probe spin density correlations between electrons with spatial resolution. This is useful since such correlations are a key property of strongly interacting electronic phases that often are difficult to measure by other means in 2D materials. One can tune several parameters in order to increase the sensitivity including the interlayer tunneling strength t_{\perp} and the layer detuning δ . As discussed above, one should however note that tuning $\delta + \epsilon_T$ close to zero to increase the signal will result in resonant exciton-electron scattering with a strong frequency dependence. Including this frequency dependence to calculate the sensitivity of our setup for resonant interactions is an interesting future problem. Another fascinating research direction is to explore the use of more than two excitons to probe higher order correlation functions. Such high order correlation functions provide deep insights into strongly correlated phases, and they are generally very hard to access by other means.

VIII. ACKNOWLEDGMENTS

This work has been supported by the Danish National Research Foundation through the Center of Excellence “CCQ” (Grant Agreement No. DNRF156). Z. W. acknowledges support from National Key R&D Program of China (Grant No. 2022YFA1404103), Natural Science Foundation of China (Grant No. 12474264) and Guangdong Provincial Quantum Science Strategic Initiative (Grant No. GDZX2404007). S.D. is also supported by the Fundamental Research Funds for the Central Universities and the National Natural Science Foundation of China (Grant No. 12404320).

Appendix A: Effects of lattice mismatches

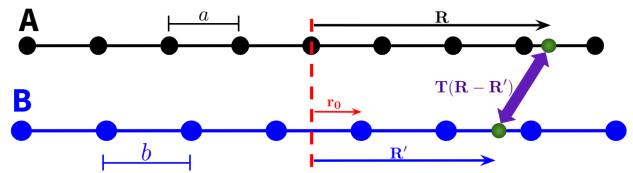


FIG. 7. Tunneling of an electron(green ball) between two chains A and B . One lattice site in chain A is chosen as the origin and the second chain is shifted relatively by an amount \mathbf{r}_0 . The amplitude for an electron at position \mathbf{R}' in chain B to tunnel to position \mathbf{R} in chain A (and vice-versa) is $T(\mathbf{R} - \mathbf{R}')$.

In this appendix, we will study how structural differences can affect the momentum of an electron tunneling between two lattices and explicitly illustrate these effects with a 1D toy-model.

We start with two lattices A and B , displaced with respect to each other by an amount \mathbf{r}_0 , as illustrated in figure 7. We assume that the tunneling amplitude for an electron in position \mathbf{R}' of lattice B to a position \mathbf{R} of the lattice A depends on their relative separation, so that the tunneling Hamiltonian reads

$$\hat{H}_t = \int_A d\mathbf{R} \int_B d\mathbf{R}' T(\mathbf{R} - \mathbf{R}') \hat{\Psi}_A^\dagger(\mathbf{R}) \hat{\Psi}_B(\mathbf{R}') + h.c. \quad (A1)$$

We express the field operators for each lattice in terms of their respective Bloch states as:

$$\hat{\Psi}_A(\mathbf{R}) = \sum_{k,m} e^{i\mathbf{k}\cdot\mathbf{R}} u_{k,m}^A(\mathbf{R}) \hat{a}_{\mathbf{k},m} \quad (A2)$$

$$\hat{\Psi}_B(\mathbf{R}') = \sum_{p,n} e^{i\mathbf{p}\cdot(\mathbf{R}' - \mathbf{r}_0)} u_{p,n}^B(\mathbf{R}' - \mathbf{r}_0) \hat{b}_{\mathbf{p},n}, \quad (A3)$$

where $\mathbf{k}(\mathbf{p})$ is a momentum inside the first Brillouin zone of $A(B)$ and $m(n)$ is a band index. In this way, the tunneling Hamiltonian takes the form

$$\hat{H}_t = \sum_{\mathbf{k}, \mathbf{p}} \sum_{m,n} T_{m,n}(\mathbf{k}, \mathbf{p}) \hat{a}_{\mathbf{k},m}^\dagger \hat{b}_{\mathbf{p},n} + h.c. \quad (A4)$$

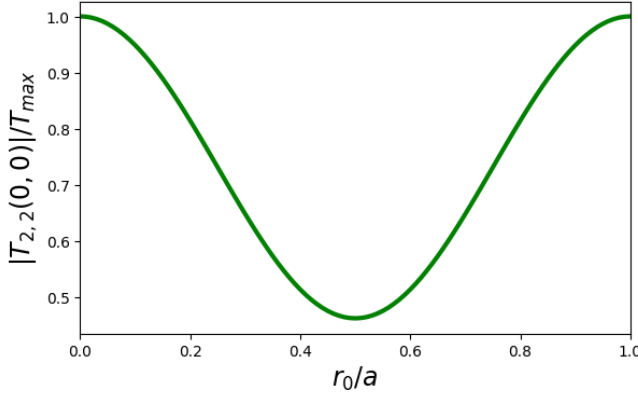


FIG. 8. Tunneling amplitude as a function of the relative displacement r_0 between two identical chains of lattice constant a . Parameters used: $\{E_0, V_a, V_b, a, b, L_A, L_B, \sigma\} = \{1, 20, 20, 1, 1, 100, 100, 0.33\}$.

with the tunneling amplitude in reciprocal space defined as

$$T_{m,n}(\mathbf{k}, \mathbf{p}) = \int_A d\mathbf{R} \int_B d\mathbf{R}' e^{i\mathbf{p} \cdot (\mathbf{R}' - \mathbf{r}_0)} e^{-i\mathbf{k} \cdot \mathbf{R}} \times (u_{\mathbf{k},m}^A(\mathbf{R}))^* u_{\mathbf{p},n}^B(\mathbf{R}' - \mathbf{r}_0) T(\mathbf{R} - \mathbf{R}'). \quad (\text{A5})$$

To illustrate the general behavior of the tunneling, we consider two one-dimensional chains modeled by sinusoidal lattice potentials for the electrons

$$\hat{H}_0^\eta = \frac{\hat{p}^2}{2m} + 2V_\eta \cos\left(\frac{2\pi}{\eta}x\right) \quad (\text{A6})$$

with $\eta = a, b$. These Hamiltonians can be diagonalized using a plain-wave basis, so that its Bloch wave functions take the form

$$u_{k,m}^\eta(x) = \sum_j c_{m,j}^\eta(k) \frac{e^{i \cdot j \cdot G^\eta x}}{\sqrt{L_\eta}} \quad (\text{A7})$$

where j is an integer, L_η is the length of each chain, $G^\eta = 2\pi/\eta$ and $c_{m,j}^\eta(k)$ are the coefficients obtained from the diagonalization of A6 for each momentum k . Plugging equation A7 in A5 and using a Gaussian ansatz for the tunneling $T(r - r') = t \exp\{-(r - r')^2/(2\sigma^2)\}$ we obtain

$$T_{m,n}(k, p) = t \sum_{j,l} \frac{(c_{m,j}^a(k))^* c_{n,l}^b(p)}{\sqrt{L_a L_b}} \int_{-L_a/2}^{L_a/2} \int_{-L_b/2+r_0}^{L_b/2+r_0} dr dr' e^{-i(k+j \cdot G^a)r} e^{i(p+l \cdot G^b)(r'-r_0)} e^{-\frac{(r-r')^2}{2\sigma^2}} \approx t \sigma \sqrt{\frac{2\pi L_a}{L_b}} \sum_{j,l} (c_{m,j}^a(k))^* c_{n,l}^b(p) e^{-p^2 \sigma^2/2} e^{-i r_0 (p+l \cdot G^b)} \text{sinc}\left(\frac{(p+l \cdot G^b) - (k+j \cdot G^a)}{2} L_a\right), \quad (\text{A8})$$

where we assume the chains are sufficiently long to obtain the explicit expression in the second line.

We first consider a scenario where two identical chains were shifted relative to each other by \mathbf{r}_0 . For numerical simulations we set $E_0 = \hbar^2/(2ma^2)$ as our unit of energy and examine the amplitude for electrons to tunnel from chain A to chain B while remaining in the same band (we chose $k = p = 0$ and the second excited band for illustration purposes). In figure 8 we see that the effect of the shift is simply to reduce the overall amplitude of the tunneling, but since the systems have the same translational invariance then in principle the momentum is not greatly affected.

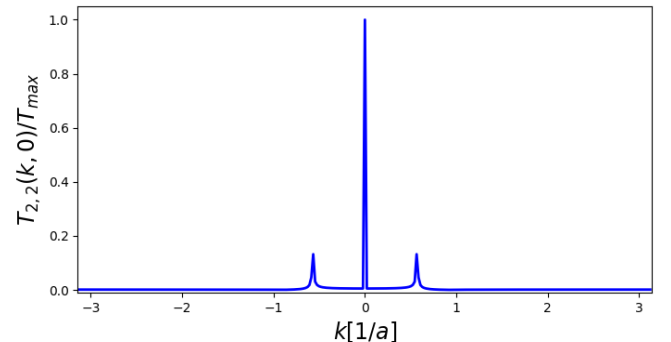


FIG. 9. Tunneling amplitudes between chains with a small lattice mismatch. Parameters used are $\{E_0, V_a, V_b, a, b, L_A, L_B, \sigma, r_0\} = \{1, 20, 16.5, 1, 1.1, 300, 330, 0.33, 0\}$.

Next, we analyze a situation of small lattice mis-

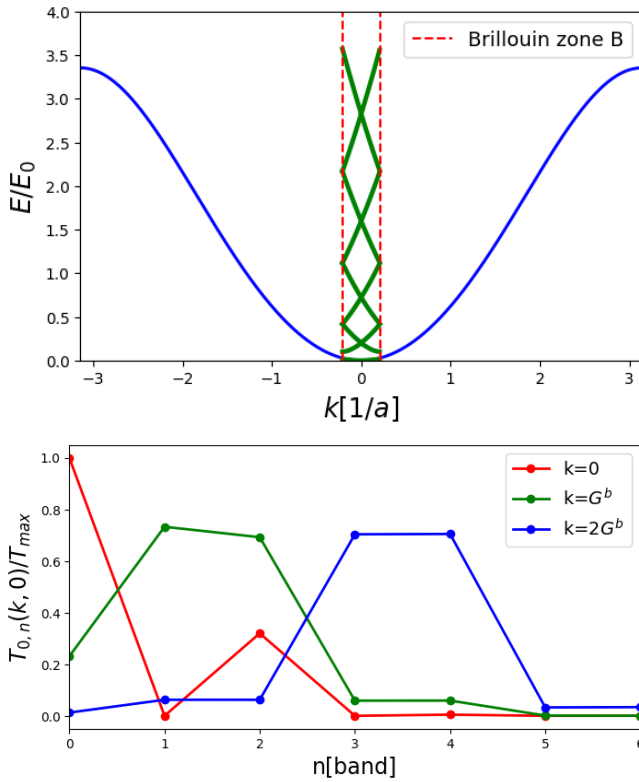


FIG. 10. **Top:** Overlapped band structures of two chains with a large mismatch. **Bottom:** Amplitudes for an electron in chain A with momentum k to tunnel to the n -th band in chain B with zero momentum. Parameters used are $\{E_0, V_a, V_b, a, b, L_A, L_B, \sigma, r_0\} = \{1, 10, 0.04, 1, 15, 1000, 1500, 0.33, 0\}$.

matches by simulating two chains with lattice constants a and $b = 1.1a$ respectively. Figure 9 shows the amplitude for electrons to tunnel from chain A to chain B at zero momentum. We see a dominant central peak, indicating momentum conservation to a large degree. However, there are two small peaks separated by a distance $\Delta k = |2\pi/a - 2\pi/b|$ from the center, which explicitly illustrate that momentum is conserved up to a difference of reciprocal lattice vectors.

Finally, we investigate a situation with large lattice mismatch. In figure 10 we set $a = 1$, $b = 15a$ and plot the band structures of the chains in their respective first Brillouin zones. It is clear that some momentum values in A can be far beyond the Brillouin zone boundaries of B .

We then calculate the tunneling amplitudes from chain A to chain B for electrons with initial momenta that were multiples of the reciprocal lattice vector of chain B ($G^b = 2\pi/b$). We conclude that high momentum electrons in lattice A will tunnel to high bands (but at small momentum) in lattice B , therefore the model in the main manuscript would need to account for these effects if, for example, the lower material in figure 1 wasn't a moiré bilayer.

Appendix B: Electron-exciton scattering matrix

Under the assumption that the low energy scattering in vacuum due to $V_{ex}(\mathbf{k})$ can be described by s -wave scattering with scattering amplitude g , one finds \mathcal{T} is only an energy ω dependent function.

$$\mathcal{T}(\omega) = g + \frac{g}{N} \sum_{\mathbf{k} \in BZ} G_U(\mathbf{k}, \omega) T(\omega) \quad (B1)$$

where BZ is the first Brillouin zone of the lattice. By solving the above equation, one has

$$\mathcal{T}(\omega) = \frac{1}{1/g - \frac{1}{N} \sum_{\mathbf{k} \in BZ} G_U(\mathbf{k}, \omega)}. \quad (B2)$$

When $\omega = \delta + \epsilon_T$, the scattering is on resonance and $\mathcal{T}(\omega)$ diverges. Consequently, one obtains the expression for g in terms of ϵ_T

$$\frac{1}{g} = \frac{1}{N} \sum_{\mathbf{k} \in BZ} G_U(\mathbf{k}, \delta + \epsilon_T) \approx \frac{1}{\epsilon_T} \quad (B3)$$

where $\epsilon_{\mathbf{k}}$ has been ignored in $G_U(\mathbf{k}, \omega)$. Therefore,

$$\begin{aligned} \mathcal{T}(\omega) &\approx \frac{1}{1/\epsilon_T - \frac{1}{\omega - \delta}} = \frac{\epsilon_T(\omega - \delta)}{\omega - \delta - \epsilon_T} \\ &\xrightarrow{\omega \ll \delta} -\frac{\epsilon_T \delta}{\omega - \delta - \epsilon_T} \\ &\xrightarrow{\omega \ll \delta + \epsilon_T} \frac{\epsilon_T \delta}{\delta + \epsilon_T}. \end{aligned} \quad (B4)$$

Appendix C: Second order energy shift

Since $G_U(\mathbf{k}, \omega)$ is approximately independent of \mathbf{k} , $\sum_{\mathbf{k}} G_U(\mathbf{k}, \omega) \exp(i\mathbf{k} \cdot \mathbf{r}) \approx 0$ for $\mathbf{r} \neq 0$. Thus one can ignore the contribution from the propagation between two excitons in upper layer to the energy shift and the second order perturbation theory gives

$$\begin{aligned}
E_2 &= \sum_{n>0} \frac{|\langle \psi_n | \hat{V}_{\text{eff}}(\mathbf{r}_1) + \hat{V}_{\text{eff}}(\mathbf{r}_2) | \psi_0 \rangle|^2}{E_0 - E_n} \\
&= \kappa^2 \sum_{n>0} \frac{\langle \psi_0 | [\hat{n}_{\sigma_1}(\mathbf{r}_1) + \hat{n}_{\sigma_2}(\mathbf{r}_2)] | \psi_n \rangle \langle \psi_n | [\hat{n}_{\sigma_1}(\mathbf{r}_1) + \hat{n}_{\sigma_2}(\mathbf{r}_2)] | \psi_0 \rangle}{E_0 - E_n} \\
&= -\kappa^2 \sum_{n>0} \frac{\langle \psi_0 | \hat{n}_{\sigma_1}(\mathbf{r}_1) | \psi_n \rangle \langle \psi_n | \hat{n}_{\sigma_1}(\mathbf{r}_1) | \psi_0 \rangle}{E_n - E_0} - \kappa^2 \sum_{n>0} \frac{\langle \psi_0 | \hat{n}_{\sigma_2}(\mathbf{r}_2) | \psi_n \rangle \langle \psi_n | \hat{n}_{\sigma_2}(\mathbf{r}_2) | \psi_0 \rangle}{E_n - E_0} \\
&\quad - \kappa^2 \sum_{n>0} \frac{\langle \psi_0 | \hat{n}_{\sigma_1}(\mathbf{r}_1) | \psi_n \rangle \langle \psi_n | \hat{n}_{\sigma_2}(\mathbf{r}_2) | \psi_0 \rangle + \langle \psi_0 | \hat{n}_{\sigma_2}(\mathbf{r}_2) | \psi_n \rangle \langle \psi_n | \hat{n}_{\sigma_1}(\mathbf{r}_1) | \psi_0 \rangle}{E_n - E_0}
\end{aligned} \tag{C1}$$

which leads to the final expression of Eq. 7 by applying the expression of the correlation function given in Ref. 45.

Appendix D: Spin-spin correlation for Eq. 10

Suppose the spin system is in the ferromagnetic phase with spin polarizing along \mathbf{x} -direction ($\phi \in [\pi/3, 2\pi/3]$). One can apply the Holstein-Primakoff transformation

$$\hat{S}_x(\mathbf{r}_i) = S - \hat{\alpha}_i^\dagger \hat{\alpha}_i \tag{D1a}$$

$$\hat{H}_2 = JS \sum_{\langle i,j \rangle} \left\{ -2 \cos(2\phi_{ij}) \hat{\alpha}_i^\dagger \hat{\alpha}_i + [\cos(2\phi_{ij}) + 1] \hat{\alpha}_i^\dagger \hat{\alpha}_j + \frac{1}{2} [\cos(2\phi_{ij}) - 1] (\hat{\alpha}_i \hat{\alpha}_j + \hat{\alpha}_i^\dagger \hat{\alpha}_j^\dagger) \right\} \tag{D4}$$

where $\phi_{ij} = -\phi_{ji}$ is applied and the linear terms in $\hat{\alpha}_i$ and $\hat{\alpha}_i^\dagger$ vanish automatically for ground state. To obtain

the excitation spectrum, we Fourier transform \hat{H}_2 into the momentum space using $\hat{\alpha}_i = (1/\sqrt{N}) \sum_{\mathbf{k}} \alpha_{\mathbf{k}} e^{i\mathbf{k}\mathbf{r}_i}$ and find

$$\hat{H}_2 = JS \sum_{\mathbf{k}} \left[A_{\mathbf{k}} \alpha_{\mathbf{k}}^\dagger \alpha_{\mathbf{k}} - \frac{1}{2} B_{\mathbf{k}} (\alpha_{\mathbf{k}} \alpha_{-\mathbf{k}} + \alpha_{\mathbf{k}}^\dagger \alpha_{-\mathbf{k}}^\dagger) \right] \tag{D5}$$

where

$$A_{\mathbf{k}} = -6 \cos(2\phi) + [\cos(2\phi) + 1] [\cos(k_x) + 2 \cos(k_x/2) \cos(\sqrt{3}k_y/2)] \tag{D6a}$$

$$B_{\mathbf{k}} = -[\cos(2\phi) - 1] [\cos k_x + 2 \cos(k_x/2) \cos(\sqrt{3}k_y/2)]. \tag{D6b}$$

With Bogoliubov approximation $\hat{\alpha}_{\mathbf{k}} = u_{\mathbf{k}} \hat{\beta}_{\mathbf{k}} + v_{\mathbf{k}} \hat{\beta}_{-\mathbf{k}}^\dagger$ and $u_{\mathbf{k}}^2 - v_{\mathbf{k}}^2 = 1$ one finds \hat{H}_2 can be diagonalized by taking

$$u_{\mathbf{k}}^2 + v_{\mathbf{k}}^2 = \frac{A_{\mathbf{k}}}{\sqrt{A_{\mathbf{k}}^2 - B_{\mathbf{k}}^2}} \tag{D7a}$$

$$2u_{\mathbf{k}}v_{\mathbf{k}} = \frac{B_{\mathbf{k}}}{\sqrt{A_{\mathbf{k}}^2 - B_{\mathbf{k}}^2}}, \tag{D7b}$$

yielding the excitation spectrum

$$E_{\mathbf{k}} = JS\sqrt{A_{\mathbf{k}}^2 - B_{\mathbf{k}}^2}. \quad (\text{D8})$$

By applying the Fourier transform $\hat{S}_z(\mathbf{k}) = (1/\sqrt{N}) \sum_i \hat{S}_z(\mathbf{r}_i) \exp(-i\mathbf{k} \cdot \mathbf{r}_i)$, the static spin-spin correlation function in momentum space reads

$$\begin{aligned} \chi_{S_z, S_z}(\mathbf{k}, 0) &= \sum_{n>0} \frac{2|\langle \psi_n | S_z(\mathbf{k}) | \psi_0 \rangle|^2}{E_n - E_0} \\ &= \sum_{n>0} \frac{2|\langle \psi_n | \frac{\sqrt{2S}}{2i} (\hat{\alpha}_{\mathbf{k}} - \hat{\alpha}_{-\mathbf{k}}^\dagger) | \psi_0 \rangle|^2}{E_n - E_0} \\ &= S \sum_{n>0} \frac{|\langle \psi_n | (v_{\mathbf{k}} \hat{\beta}_{-\mathbf{k}}^\dagger - u_{\mathbf{k}} \hat{\beta}_{-\mathbf{k}}^\dagger) | \psi_0 \rangle|^2}{E_n - E_0} \\ &= \frac{1}{J(A_{\mathbf{k}} + B_{\mathbf{k}})}. \end{aligned} \quad (\text{D9})$$

As a result, the spin-spin correlation in real space is given by

$$\begin{aligned} \langle \langle \hat{S}_z(\mathbf{r}_i), \hat{S}_z(\mathbf{r}_j) \rangle \rangle &= \frac{1}{N} \sum_{\mathbf{k}} \chi_{S_z, S_z}(\mathbf{k}, 0) e^{i\mathbf{k} \cdot (\mathbf{r}_i - \mathbf{r}_j)} \\ &= \frac{1}{NJ} \sum_{\mathbf{k}} \frac{e^{i\mathbf{k} \cdot (\mathbf{r}_i - \mathbf{r}_j)}}{A_{\mathbf{k}} + B_{\mathbf{k}}}. \end{aligned} \quad (\text{D10})$$

If the system is in the 120° -1 (120° -2) antiferromagnetic order, that is $\phi \in [2\pi/3, \pi]$ ($[0, \pi/3]$), one can first express the Hamiltonian in terms of the spin in the frame rotated around \hat{z} -axis by angle $\theta_i = \mathbf{Q} \cdot \mathbf{r}_i$ with $\mathbf{Q} = (-4\pi/3, 0)$ ($\mathbf{Q} = (4\pi/3, 0)$) and then treat the system in the rotated frame as the ferromagnetic order and apply the Holstein-Primakoff transformation shown in Eq. D1 to calculate the spin-spin correlation function. Now we only perform explicit calculations for the 120° -1 antiferromagnetic order, as that for the 120° -2 antiferromagnetic order is similar. The relationship between the spin in laboratory frame (S_x, S_y, S_z) and rotational frame (S_x^R, S_y^R, S_z^R) is

$$\hat{S}_x = \hat{S}_x^R \cos \theta - \hat{S}_y^R \sin \theta \quad (\text{D11a})$$

$$\hat{S}_y = \hat{S}_x^R \sin \theta + \hat{S}_y^R \cos \theta \quad (\text{D11b})$$

$$\hat{S}_z = \hat{S}_z^R. \quad (\text{D11c})$$

Therefore, the Hamiltonian in the rotated frame is

$$\begin{aligned} \hat{H}_S &= J \sum_{\langle i,j \rangle} \left\{ \hat{S}_z^R(\mathbf{r}_i) \hat{S}_z^R(\mathbf{r}_j) + \cos(\theta_i - \theta_j + 2\phi_{ij}) \left[\hat{S}_x^R(\mathbf{r}_i) \hat{S}_x^R(\mathbf{r}_j) + \hat{S}_y^R(\mathbf{r}_i) \hat{S}_y^R(\mathbf{r}_j) \right] \right. \\ &\quad \left. + \sin(\theta_i - \theta_j + 2\phi_{ij}) \left[\hat{S}_x^R(\mathbf{r}_i) \hat{S}_y^R(\mathbf{r}_j) - \hat{S}_y^R(\mathbf{r}_i) \hat{S}_x^R(\mathbf{r}_j) \right] \right\}. \end{aligned} \quad (\text{D12})$$

Compared to Eq. 10, this Hamiltonian has only two differences: 1) $\hat{S}_{x,y,z}(\mathbf{r}_i)$ is replaced by $\hat{S}_{x,y,z}^R(\mathbf{r}_i)$, and 2) $2\phi_{ij}$ is replaced by $\theta_i - \theta_j + 2\phi_{ij}$. Since $\theta_i - \theta_j = -(\theta_j - \theta_i)$, the dummy variable can be exchanged as in deriving Eq. D2, and one can easily write down the Hamiltonian after performing the Holstein-Primakoff transformation given

in Eq. D1 (replacing $\hat{S}_{x,y,z}(\mathbf{r}_i)$ by $\hat{S}_{x,y,z}^R(\mathbf{r}_i)$). That is

$$\hat{H}_S = \hat{H}_0 + \hat{H}_2 \quad (\text{D13})$$

where

$$\begin{aligned} \hat{H}_0 &= JS^2 \sum_{\langle i,j \rangle} \cos(\theta_i - \theta_j + 2\phi_{ij}) \\ &= 3NJS^2 \cos\left(2\phi - \frac{2\pi}{3}\right) \end{aligned} \quad (\text{D14})$$

and

$$\hat{H}_2 = JS \sum_{\langle i,j \rangle} \left\{ -2 \cos(\theta_i - \theta_j + 2\phi_{ij}) \hat{a}_i^\dagger \hat{a}_i + [\cos(\theta_i - \theta_j + 2\phi_{ij}) + 1] \hat{a}_i^\dagger \hat{a}_j + \frac{1}{2} [\cos(\theta_i - \theta_j + 2\phi_{ij}) - 1] (\hat{a}_i \hat{a}_j + \hat{a}_i^\dagger \hat{a}_j^\dagger) \right\}. \quad (\text{D15})$$

Fourier transform H_2 to momentum space, one obtains Eq. D5 with

$$A_{\mathbf{k}} = -6 \cos(2\phi - \frac{2\pi}{3}) + \left[\cos\left(2\phi - \frac{2\pi}{3}\right) + 1 \right] \left[\cos(k_x) + 2 \cos(k_x/2) \cos(\sqrt{3}k_y/2) \right] \quad (\text{D16a})$$

and

$$B_{\mathbf{k}} = - \left[\cos\left(2\phi - \frac{2\pi}{3}\right) - 1 \right] \left[\cos k_x + 2 \cos(k_x/2) \cos(\sqrt{3}k_y/2) \right]. \quad (\text{D16b})$$

These expressions can be obtained by shifting ϕ by $\pi/3$ in those for the ferromagnetic order. Therefore, the spin-spin correlation function is same as that for the ferromagnetic order except for a shift of ϕ by $\pi/3$. Similarly, one can verify that the spin-spin correlation function for 120°-2 antiferromagnetic order is also same as that for ferromagnetic order except a shift of ϕ by $-\pi/3$.

Appendix E: Spin correlations for a superconducting sample

In this appendix we derive the correlation functions for a Hamiltonian which is more general than the one shown in the main text. Following generalized BCS theory, it is well known that the single-band BdG Hamiltonian can be diagonalized as

$$\begin{aligned} \hat{H} &= \frac{1}{2} \sum_{\mathbf{k}} \hat{\Psi}_k^\dagger \begin{pmatrix} \xi_{\mathbf{k}} \hat{\sigma}_0 & \hat{\Delta}_{\mathbf{k}} \\ \hat{\Delta}_{\mathbf{k}}^\dagger & -\xi_{\mathbf{k}} \hat{\sigma}_0 \end{pmatrix} \hat{\Psi}_{\mathbf{k}} + \text{const} \\ &= \sum_{\mathbf{k}} E_{\mathbf{k}} (\gamma_{\mathbf{k}\uparrow}^\dagger \gamma_{\mathbf{k}\uparrow} + \gamma_{\mathbf{k}\downarrow}^\dagger \gamma_{\mathbf{k}\downarrow}). \end{aligned} \quad (\text{E1})$$

Here $\hat{\Psi}_{\mathbf{k}} := (\hat{c}_{\mathbf{k}\uparrow}, \hat{c}_{\mathbf{k}\downarrow}, \hat{c}_{-\mathbf{k}\uparrow}^\dagger, \hat{c}_{-\mathbf{k}\downarrow}^\dagger)^T$ is the Nambu vector, $\hat{\Delta}_{\mathbf{k}}$ is the gap function matrix, (which includes pairing amplitudes between electrons with both parallel and anti-parallel spins), and $\hat{\Gamma}_{\mathbf{k}} = (\gamma_{\mathbf{k}\uparrow}, \gamma_{\mathbf{k}\downarrow}, \gamma_{-\mathbf{k}\uparrow}^\dagger, \gamma_{-\mathbf{k}\downarrow}^\dagger)$ are the Bogoliubov quasi-particle operators, which are related to the electronic operators by the unitary transformation

$$\hat{\Psi}_{\mathbf{k}} = \hat{U}_{\mathbf{k}} \hat{\Gamma}_{\mathbf{k}}, \quad \hat{U}_{\mathbf{k}} := \begin{pmatrix} \hat{u}_{\mathbf{k}} & \hat{v}_{\mathbf{k}} \\ \hat{v}_{-\mathbf{k}}^* & \hat{u}_{-\mathbf{k}}^* \end{pmatrix}. \quad (\text{E2})$$

For unitary pairing, the transformation takes a simplified form⁴⁶

$$\hat{u}_{\mathbf{k}} = \frac{E_{\mathbf{k}} + \xi_{\mathbf{k}}}{\sqrt{2E_{\mathbf{k}}(E_{\mathbf{k}} + \xi_{\mathbf{k}})}} \hat{\sigma}_0, \quad \hat{v}_{\mathbf{k}} = \frac{-1}{\sqrt{2E_{\mathbf{k}}(E_{\mathbf{k}} + \xi_{\mathbf{k}})}} \hat{\Delta}_{\mathbf{k}}, \quad (\text{E3})$$

where $E_{\mathbf{k}} = \sqrt{\xi_{\mathbf{k}}^2 + |\Delta_{\mathbf{k}}|^2}$. Using the transformations E2 we can express the operators in equation 5 in terms of the quasi-particle operators as

$$\begin{aligned} \hat{c}_{\mathbf{p}\sigma}^\dagger \hat{c}_{\mathbf{q}\sigma} &= u_{\mathbf{p}} u_{\mathbf{q}} \gamma_{\mathbf{p}\sigma}^\dagger \gamma_{\mathbf{q}\sigma} + v_{\mathbf{p};\sigma\sigma}^* v_{\mathbf{q};\sigma\sigma} \gamma_{-\mathbf{p}\sigma} \gamma_{-\mathbf{q}\sigma}^\dagger \\ &+ v_{\mathbf{p};\sigma\sigma}^* v_{\mathbf{q};\sigma-\sigma} \gamma_{-\mathbf{p}\sigma} \gamma_{-\mathbf{q}-\sigma}^\dagger + v_{\mathbf{p};\sigma-\sigma}^* v_{\mathbf{q};\sigma\sigma} \gamma_{-\mathbf{p}-\sigma} \gamma_{-\mathbf{q}\sigma}^\dagger \\ &+ v_{\mathbf{p};\sigma-\sigma}^* v_{\mathbf{q};\sigma-\sigma} \gamma_{-\mathbf{p}-\sigma} \gamma_{-\mathbf{q}-\sigma}^\dagger - u_{\mathbf{p}} v_{\mathbf{q};\sigma\sigma} \gamma_{\mathbf{p}\sigma} \gamma_{-\mathbf{q}\sigma}^\dagger \\ &- u_{\mathbf{p}} v_{\mathbf{q};\sigma-\sigma} \gamma_{\mathbf{p}\sigma}^\dagger \gamma_{-\mathbf{q}-\sigma}^\dagger - v_{\mathbf{p};\sigma\sigma}^* u_{\mathbf{q}} \gamma_{-\mathbf{p}\sigma} \gamma_{\mathbf{q}\sigma} \\ &- v_{\mathbf{p};\sigma-\sigma}^* u_{\mathbf{q}} \gamma_{-\mathbf{p}-\sigma} \gamma_{\mathbf{q}\sigma}. \end{aligned} \quad (\text{E4})$$

The previous expression allows us to explicitly compute the matrix elements of density operators $\hat{n}_{\mathbf{r},\sigma}$. We now assume that the superconducting ground-state has no Bogoliubov quasi-particles so that $\gamma_{\mathbf{k}\sigma} |\psi_0\rangle = 0$ and $\langle\psi_0|\gamma_{\mathbf{k}\sigma}\gamma_{\mathbf{k}'\sigma'}^\dagger|\psi_0\rangle = \delta_{\mathbf{k},\mathbf{k}'}\delta_{\sigma,\sigma'}$. From the previous analysis, we find that the only excited states that will yield non-vanishing matrix elements $\langle\psi_0|\hat{n}_{\mathbf{r}\sigma}|\psi\rangle$ are those of the form $|\psi\rangle = |\mathbf{k},\sigma; \mathbf{k}',\sigma'\rangle := \gamma_{\mathbf{k}\sigma}^\dagger \gamma_{\mathbf{k}'\sigma'}^\dagger |\psi_0\rangle$, therefore we obtain

$$\begin{cases} \langle\psi_0|\hat{n}_{\mathbf{r},\downarrow}|\mathbf{k},\downarrow; \mathbf{k}',\uparrow\rangle &= -\frac{1}{N} e^{i(\mathbf{k}+\mathbf{k}')\cdot\mathbf{r}} v_{-\mathbf{k}',\downarrow\uparrow}^* u_{\mathbf{k}} \\ \langle\psi_0|\hat{n}_{\mathbf{r},\downarrow}|\mathbf{k},\downarrow; \mathbf{k}',\downarrow\rangle &= \frac{-1}{N} e^{i(\mathbf{k}+\mathbf{k}')\cdot\mathbf{r}} (u_{\mathbf{k}} v_{-\mathbf{k}',\downarrow\downarrow}^* - u_{\mathbf{k}'} v_{-\mathbf{k},\downarrow\downarrow}^*) \\ \langle\psi_0|\hat{n}_{\mathbf{r},\uparrow}|\mathbf{k},\downarrow; \mathbf{k}',\uparrow\rangle &= \frac{1}{N} e^{i(\mathbf{k}+\mathbf{k}')\cdot\mathbf{r}} v_{-\mathbf{k},\uparrow\downarrow}^* u_{\mathbf{k}'} \\ \langle\psi_0|\hat{n}_{\mathbf{r},\downarrow}|\mathbf{k},\uparrow; \mathbf{k}',\uparrow\rangle &= 0 \\ \langle\psi_0|\hat{n}_{\mathbf{r},\uparrow}|\mathbf{k},\downarrow; \mathbf{k}',\downarrow\rangle &= 0. \end{cases}$$

Since the excited states are pairs of Bogoliubons with different momenta and spins, equation 7 for a superconductor turns into a double sum over \mathbf{k} and \mathbf{k}' . Starting with the parallel-spin correlation, we need to be careful with double counting over some states, because $|\mathbf{k},\downarrow; \mathbf{k}',\downarrow\rangle = -|\mathbf{k}',\downarrow; \mathbf{k},\downarrow\rangle$. This is easily resolved by adding a factor of 1/2 wherever necessary, that is

$$\begin{aligned}
& \langle\langle \hat{n}_\downarrow(\mathbf{r}), \hat{n}_\downarrow(\mathbf{0}) \rangle\rangle \\
&= \frac{1}{2} \sum_{\mathbf{k}, \mathbf{k}'} \frac{\langle \mathbf{k}, \downarrow; \mathbf{k}', \downarrow | \hat{n}_{\mathbf{r}, \downarrow} | \psi_0 \rangle \langle \psi_0 | \hat{n}_{\mathbf{0}, \downarrow} | \mathbf{k}, \downarrow; \mathbf{k}', \downarrow \rangle + c.c.}{E_{\mathbf{k}} + E_{\mathbf{k}'}} + \sum_{\mathbf{k}, \mathbf{k}'} \frac{\langle \mathbf{k}, \downarrow; \mathbf{k}', \uparrow | \hat{n}_{\mathbf{r}, \downarrow} | \psi_0 \rangle \langle \psi_0 | \hat{n}_{\mathbf{0}, \downarrow} | \mathbf{k}, \downarrow; \mathbf{k}', \uparrow \rangle + c.c.}{E_{\mathbf{k}} + E_{\mathbf{k}'}} \\
&= \frac{1}{2N^2} \sum_{\mathbf{k}, \mathbf{k}'} \frac{e^{-i(\mathbf{k}+\mathbf{k}') \cdot \mathbf{r}} (u_{\mathbf{k}}^* v_{-\mathbf{k}'; \downarrow\downarrow} - u_{\mathbf{k}'}^* v_{-\mathbf{k}; \downarrow\downarrow}) (u_{\mathbf{k}} v_{-\mathbf{k}'; \downarrow\downarrow}^* - u_{\mathbf{k}'} v_{-\mathbf{k}; \downarrow\downarrow}^*) + c.c.}{E_{\mathbf{k}} + E_{\mathbf{k}'}} + \frac{1}{N^2} \sum_{\mathbf{k}, \mathbf{k}'} \frac{e^{-i(\mathbf{k}+\mathbf{k}') \cdot \mathbf{r}} |u_{\mathbf{k}}|^2 |v_{-\mathbf{k}'; \downarrow\uparrow}|^2 + c.c.}{E_{\mathbf{k}} + E_{\mathbf{k}'}} \\
&= \frac{2}{N^2} \sum_{\mathbf{k}, \mathbf{k}'} \frac{|u_{\mathbf{k}}|^2 (|v_{-\mathbf{k}'; \downarrow\uparrow}|^2 + |v_{\mathbf{k}'; \downarrow\downarrow}|^2)}{E_{\mathbf{k}} + E_{\mathbf{k}'}} \cos((\mathbf{k} + \mathbf{k}') \cdot \mathbf{r}) - \frac{2}{N^2} \sum_{\mathbf{k}, \mathbf{k}'} \frac{(u_{\mathbf{k}} v_{-\mathbf{k}; \downarrow\downarrow})^* (u_{\mathbf{k}'} v_{-\mathbf{k}'; \downarrow\downarrow}) e^{-i(\mathbf{k}+\mathbf{k}') \cdot \mathbf{r}}}{E_{\mathbf{k}} + E_{\mathbf{k}'}}. \tag{E5}
\end{aligned}$$

In the last step, we used summation over dummy indices to group similar terms. The expression can be further simplified if we recall the explicit form of the transformations E3 and see that

$$\begin{aligned}
u_{\mathbf{k}} v_{-\mathbf{k}; \sigma\sigma'} &= \left(\frac{E_{\mathbf{k}} + \xi_{\mathbf{k}}}{\sqrt{2E_{\mathbf{k}}(E_{\mathbf{k}} + \xi_{\mathbf{k}})}} \right) \left(\frac{-\Delta_{-\mathbf{k}; \sigma\sigma'}}{\sqrt{2E_{\mathbf{k}}(E_{\mathbf{k}} + \xi_{\mathbf{k}})}} \right) \\
&= -\frac{\Delta_{-\mathbf{k}, \sigma\sigma'}}{2E_{\mathbf{k}}}. \tag{E6}
\end{aligned}$$

Plugging E6 in E5, and using the anti-symmetry property of the gap function matrix $\hat{\Delta}_{\mathbf{k}} = -\hat{\Delta}_{-\mathbf{k}}$, the parallel spin correlation takes the form

$$\langle\langle \hat{n}_\downarrow(\mathbf{r}), \hat{n}_\downarrow(\mathbf{0}) \rangle\rangle = \frac{2}{N^2} \sum_{\mathbf{k}, \mathbf{k}'} \frac{|u_{\mathbf{k}}|^2 |v_{\mathbf{k}'}|^2}{E_{\mathbf{k}} + E_{\mathbf{k}'}} \cos((\mathbf{k} + \mathbf{k}') \cdot \mathbf{r}) + \frac{1}{2N^2} \sum_{\mathbf{k}, \mathbf{k}'} \frac{1}{E_{\mathbf{k}} + E_{\mathbf{k}'}} \frac{e^{-i(\mathbf{k}+\mathbf{k}') \cdot \mathbf{r}}}{E_{\mathbf{k}} E_{\mathbf{k}'}} \Delta_{\mathbf{k}; \downarrow\downarrow}^* \Delta_{-\mathbf{k}', \downarrow\downarrow}.$$

For the antiparallel spin correlation $\langle\langle \hat{n}_\downarrow(\mathbf{r}), \hat{n}_\uparrow(\mathbf{0}) \rangle\rangle$, the matrix elements involving pairs of Bogoliubons with the same spin yield no contributions, therefore we sum over

the states with pairs Bogoliubons of opposite spins. Using this fact, and recalling equation E6 and the anti-symmetry of the cooper-pair matrix, we get

$$\begin{aligned}
& \langle\langle \hat{n}_\downarrow(\mathbf{r}), \hat{n}_\uparrow(\mathbf{0}) \rangle\rangle = \sum_{\mathbf{k}, \mathbf{k}'} \frac{1}{E_{\mathbf{k}} + E_{\mathbf{k}'}} (\langle \mathbf{k}, \downarrow; \mathbf{k}' \uparrow | \hat{n}_{\mathbf{r}, \uparrow} | \psi_0 \rangle \langle \psi_0 | \hat{n}_{\mathbf{0}, \downarrow} | \mathbf{k}, \downarrow; \mathbf{k}' \uparrow \rangle + c.c.) \\
&= \frac{-1}{N^2} \sum_{\mathbf{k}, \mathbf{k}'} \frac{1}{E_{\mathbf{k}} + E_{\mathbf{k}'}} \left(e^{-i(\mathbf{k}+\mathbf{k}') \cdot \mathbf{r}} v_{-\mathbf{k}, \uparrow\downarrow} u_{\mathbf{k}} v_{-\mathbf{k}', \uparrow\downarrow}^* + c.c. \right) \\
&= -\frac{1}{4N^2} \sum_{\mathbf{k}, \mathbf{k}'} \frac{1}{E_{\mathbf{k}} + E_{\mathbf{k}'}} \frac{1}{E_{\mathbf{k}} E_{\mathbf{k}'}} \left(e^{-i(\mathbf{k}+\mathbf{k}') \cdot \mathbf{r}} \Delta_{-\mathbf{k}, \uparrow\downarrow} \Delta_{-\mathbf{k}', \uparrow\downarrow}^* + e^{i(\mathbf{k}+\mathbf{k}') \cdot \mathbf{r}} \Delta_{-\mathbf{k}, \uparrow\downarrow}^* \Delta_{-\mathbf{k}', \uparrow\downarrow} \right) \\
&= \frac{1}{4N^2} \sum_{\mathbf{k}, \mathbf{k}'} \frac{1}{E_{\mathbf{k}} + E_{\mathbf{k}'}} \frac{e^{-i(\mathbf{k}+\mathbf{k}') \cdot \mathbf{r}}}{E_{\mathbf{k}} E_{\mathbf{k}'}} \Delta_{-\mathbf{k}, \uparrow\downarrow} \Delta_{-\mathbf{k}', \uparrow\downarrow}^* + \frac{1}{4N^2} \sum_{\mathbf{k}, \mathbf{k}'} \frac{1}{E_{\mathbf{k}} + E_{\mathbf{k}'}} \frac{e^{-i(\mathbf{k}+\mathbf{k}') \cdot \mathbf{r}}}{E_{\mathbf{k}} E_{\mathbf{k}'}} \Delta_{\mathbf{k}, \uparrow\downarrow}^* \Delta_{-\mathbf{k}', \uparrow\downarrow} \\
&= \frac{1}{2N^2} \sum_{\mathbf{k}, \mathbf{k}'} \frac{1}{E_{\mathbf{k}} + E_{\mathbf{k}'}} \frac{e^{-i(\mathbf{k}+\mathbf{k}') \cdot \mathbf{r}}}{E_{\mathbf{k}} E_{\mathbf{k}'}} \Delta_{-\mathbf{k}, \uparrow\downarrow} \Delta_{\mathbf{k}', \uparrow\downarrow}^*. \tag{E7}
\end{aligned}$$

This is the correlation function studied in section VI.

¹ G. Wang, A. Chernikov, M. M. Glazov, T. F. Heinz, X. Marie, T. Amand, and B. Urbaszek, *Rev. Mod. Phys.* **90**, 021001 (2018).

² K. F. Mak, K. He, J. Shan, and T. F. Heinz, *Nature Nanotechnology* **7**, 494 (2012).

³ H. Zeng, J. Dai, W. Yao, D. Xiao, and X. Cui, *Nature Nanotechnology* **7**, 490 (2012).

⁴ R. Bistritzer and A. H. MacDonald, *Proceedings of the National Academy of Sciences* **108**, 12233 (2011), <https://www.pnas.org/doi/pdf/10.1073/pnas.1108174108>.

⁵ F. Wu, T. Lovorn, E. Tutuc, and A. H. MacDonald, *Physical review letters* **121**, 026402 (2018).

⁶ H. Pan, F. Wu, and S. D. Sarma, *Physical Review Research* **2**, 033087 (2020).

⁷ J. Zang, J. Wang, J. Cano, and A. J. Millis, *Physical Review B* **104**, 075150 (2021).

⁸ K. F. Mak and J. Shan, *Nature Nanotechnology* **17**, 686 (2022).

⁹ A. G. Salvador, C. Kuhlenkamp, L. Ciorciaro, M. Knap, and A. İmamoğlu, *Physical Review Letters* **128**, 237401 (2022).

¹⁰ T. Smoleński, P. E. Dolgirev, C. Kuhlenkamp, A. Popert, Y. Shimazaki, P. Back, X. Lu, M. Kroner, K. Watanabe, T. Taniguchi, I. Esterlis, E. Demler, and A. İmamoğlu, *Nature* **595**, 53 (2021).

¹¹ Y. Shimazaki, C. Kuhlenkamp, I. Schwartz, T. Smoleński, K. Watanabe, T. Taniguchi, M. Kroner, R. Schmidt, M. Knap, and A. m. c. İmamoğlu, *Phys. Rev. X* **11**, 021027 (2021).

¹² L. Ciorciaro, T. Smoleński, I. Morera, N. Kiper, S. Hiesstand, M. Kroner, Y. Zhang, K. Watanabe, T. Taniguchi, E. Demler, and A. İmamoğlu, *Nature* **623**, 509 (2023).

¹³ C. Jin, Z. Tao, T. Li, Y. Xu, Y. Tang, J. Zhu, S. Liu, K. Watanabe, T. Taniguchi, J. C. Hone, L. Fu, J. Shan, and K. F. Mak, *Nature Materials* **20**, 940 (2021).

¹⁴ Y. Xu, S. Liu, D. A. Rhodes, K. Watanabe, T. Taniguchi, J. Hone, V. Elser, K. F. Mak, and J. Shan, *Nature* **587**, 214 (2020).

¹⁵ S. Miao, T. Wang, X. Huang, D. Chen, Z. Lian, C. Wang, M. Blei, T. Taniguchi, K. Watanabe, S. Tongay, Z. Wang, D. Xiao, Y.-T. Cui, and S.-F. Shi, *Nature Communications* **12**, 3608 (2021).

¹⁶ Y. Zhou, J. Sung, E. Brutschea, I. Esterlis, Y. Wang, G. Scuri, R. J. Gelly, H. Heo, T. Taniguchi, K. Watanabe, G. Zaránd, M. D. Lukin, P. Kim, E. Demler, and H. Park, *Nature* **595**, 48 (2021).

¹⁷ H. Cui, Q. Hu, X. Zhao, L. Ma, F. Jin, Q. Zhang, K. Watanabe, T. Taniguchi, J. Shan, K. F. Mak, Y. Li, and Y. Xu, *Nano Letters* **24**, 7077 (2024).

¹⁸ T. Smoleński, O. Cotlet, A. Popert, P. Back, Y. Shimazaki, P. Knüppel, N. Dietler, T. Taniguchi, K. Watanabe, M. Kroner, and A. İmamoğlu, *Phys. Rev. Lett.* **123**, 097403 (2019).

¹⁹ J. Gu, L. Ma, S. Liu, K. Watanabe, T. Taniguchi, J. C. Hone, J. Shan, and K. F. Mak, *Nature Physics* **18**, 395 (2022).

²⁰ G. Mazza and A. Amariucci, *Phys. Rev. B* **106**, L241104 (2022).

²¹ A. Julku, S. Ding, and G. M. Bruun, *Phys. Rev. Res.* **6**, 033119 (2024).

²² T.-S. Huang, Y.-Z. Chou, C. L. Baldwin, F. Wu, and M. Hafezi, *Phys. Rev. B* **107**, 195151 (2023).

²³ I. Amelio, N. D. Drummond, E. Demler, R. Schmidt, and A. İmamoğlu, *Phys. Rev. B* **107**, 155303 (2023).

²⁴ A. K. Sorout, S. Sarkar, and S. Gangadharaiah, *Journal of Physics: Condensed Matter* **32**, 415604 (2020).

²⁵ P. Massignan, R. Schmidt, G. E. Astrakharchik, A. İmamoğlu, M. Zwierlein, J. J. Arlt, and G. M. Bruun, “Polarons in atomic gases and two-dimensional semiconductors,” (2025), arXiv:2501.09618 [cond-mat.quant-gas].

²⁶ I. Schwartz, Y. Shimazaki, C. Kuhlenkamp, K. Watanabe, T. Taniguchi, M. Kroner, and A. İmamoğlu, *Science* **374**, 336 (2021).

²⁷ K. L. Seyler, P. Rivera, H. Yu, N. P. Wilson, E. L. Ray, D. G. Mandrus, J. Yan, W. Yao, and X. Xu, *Nature* **567**, 66 (2019).

²⁸ W. Li, X. Lu, S. Dubey, L. Devenica, and A. Srivastava, *Nature materials* **19**, 624 (2020).

²⁹ M. Brotons-Gisbert, H. Baek, A. Molina-Sánchez, A. Campbell, E. Scerri, D. White, K. Watanabe, T. Taniguchi, C. Bonato, and B. D. Gerardot, *Nature Materials* **19**, 630 (2020).

³⁰ M. Brotons-Gisbert, H. Baek, A. Campbell, K. Watanabe, T. Taniguchi, and B. D. Gerardot, *Physical Review X* **11**, 031033 (2021).

³¹ H. Baek, M. Brotons-Gisbert, A. Campbell, V. Vitale, J. Lischner, K. Watanabe, T. Taniguchi, and B. D. Gerardot, *Nature Nanotechnology* **16**, 1237 (2021).

³² E. Liu, E. Barré, J. van Baren, M. Wilson, T. Taniguchi, K. Watanabe, Y.-T. Cui, N. M. Gabor, T. F. Heinz, Y.-C. Chang, *et al.*, *Nature* **594**, 46 (2021).

³³ C. Kuhlenkamp, M. Knap, M. Wagner, R. Schmidt, and A. İmamoğlu, *Physical Review Letters* **129**, 037401 (2022).

³⁴ S. Ding, M. Drewsen, J. J. Arlt, and G. M. Bruun, *Phys. Rev. Lett.* **129**, 153401 (2022).

³⁵ R. Paredes, G. Bruun, and A. Camacho-Guardian, *Phys. Rev. A* **110**, 030101 (2024).

³⁶ A. Auerbach, *Interacting Electrons and Quantum Magnetism*, Graduate Texts in Contemporary Physics (Springer New York, 2012).

³⁷ M. A. Ruderman and C. Kittel, *Physical Review* **96**, 99 (1954).

³⁸ T. Kasuya, *Progress of theoretical physics* **16**, 45 (1956).

³⁹ K. Yosida, *Physical Review* **106**, 893 (1957).

⁴⁰ Y. Tang, L. Li, T. Li, Y. Xu, S. Liu, K. Barmak, K. Watanabe, T. Taniguchi, A. H. MacDonald, J. Shan, *et al.*, *Nature* **579**, 353 (2020).

⁴¹ Y. Zhou, K. Kanoda, and T.-K. Ng, *Reviews of Modern Physics* **89**, 025003 (2017).

⁴² E. Pangburn, L. Haurie, A. Crépieux, O. A. Awoga, A. M. Black-Schaffer, C. Pépin, and C. Bena, *Phys. Rev. B* **108**, 134514 (2023).

⁴³ Y. Xia, Z. Han, K. Watanabe, T. Taniguchi, J. Shan, and K. F. Mak, *Nature* **637**, 833 (2025).

⁴⁴ Y. Cao, V. Fatemi, S. Fang, K. Watanabe, T. Taniguchi, E. Kaxiras, and P. Jarillo-Herrero, *Nature* **556**, 43 (2018).

⁴⁵ L. Pitaevskii and S. Stringari, *Bose-Einstein condensation and superfluidity*, Vol. 164 (Oxford University Press, 2016).

⁴⁶ M. Sigrist, *Introduction to Unconventional Superconductivity*, Vol. 789 (AIP publishing, 2005) pp. 165–243.